# P9.4 A SENSITIVITY STUDY OF THE OPERATIONAL NSSL WRF USING UNIQUE NASA ASSETS

Jonathan L. Case[1], Scott R. Dembek[2], John S. Kain[3], Sujay V. Kumar[4], Toshihisa Matsui[4], Jainn J. Shi[4], William M. Lapenta[5], and Wei-Kuo Tao[6]

[1]ENSCO Inc./Short-term Prediction Research and Transition (SPoRT) Center
[2]Universities Space Research Association/SPoRT Center, Huntsville, AL
[3]NOAA/National Severe Storms Laboratory, Norman, OK
[4]Goddard Earth Sciences and Technology Center, Greenbelt, MD
[5]NASA Marshall Space Flight Center/SPoRT Center, Huntsville, AL
[6]NASA Goddard Space Flight Center, Laboratory for Atmospheres, Greenbelt, MD

## 1. INTRODUCTION

The NASA Short-term Prediction Research and Transition (SPoRT) Center has teamed with the NOAA/National Severe Storms Laboratory (NSSL) to conduct simulation experiments of the operational NSSL runs in post-analysis mode for several severe weather episodes from the 2007 and 2008 Spring Experiments. Through these sensitivity runs, the SPoRT Center seeks to demonstrate the potential added value of NASA products developed by the Goddard Space Flight Center (GSFC) and the SPoRT Center to the Advanced Research WRF (ARW) model. These contributions include short- and long-wave radiation schemes, a 3-ice microphysics scheme, and high-resolution lower boundary data from the NASA Land Information System (LIS; Kumar *et al.* 2006, 2007) to spin-up and initialize the land surface variables. In addition, a SPoRT Center high-resolution sea surface temperature (SST) composite derived from the Moderate Resolution Imaging Spectroradiometer (MODIS) instruments aboard the Aqua and Terra satellites is used in some simulations.

NSSL has been running a real-time configuration of the ARW model with explicit convective forecasts since 2006. These forecasts have provided the focal point for close interaction and collaboration between research scientists and operational forecasters in both Norman, OK and Huntsville, AL.

This paper/poster presentation focuses on preliminary results and assessments of sensitivity runs from the 2007 Spring Experiment. The remainder of this paper is organized as follows. Background information on the NASA SPoRT Center is provided in Section 2. Section 3 describes the Hazardous Weather Testbed Spring Experiments and the collaboration between the SPoRT Center and NSSL. Section 4 provides a brief description of the operational NSSL WRF configuration. The suite of sensitivity experiments to test the impacts of unique NASA contributions to WRF is given in Section 5. Preliminary results are presented in Section 6. A summary and future collaborative work are presented in Section 7 with acknowledgements and references given in Sections 8 and 9, respectively.

## 2. THE NASA SPORT CENTER

The NASA SPoRT program at the Marshall Space Flight Center (MSFC) seeks to accelerate the infusion of NASA Earth Science observations, data assimilation, and modeling research into weather forecast operations and decision-making at the regional and local level. It directly supports the NASA strategic plan of using results of scientific discovery to directly benefit society. The program is executed in concert with other government, university, and private sector partners. The primary focus is on the regional scale and emphasizes forecast improvements on a time scale of 0-24 hours. The SPoRT program has facilitated the use of real-time NASA data and products to 13 National Weather Service (NWS) Weather Forecast Offices (WFOs) and several private weather entities primarily in the southeast United States. Numerous new techniques have been developed to transform satellite observations into useful parameters that better describe changing weather conditions.

The unique weather products have helped local weather service offices improve forecasts of reduced visibility due to fog, low clouds, and smoke and haze from sources such as forest fires and agricultural burning, the onset of precipitation, the occurrence and location of severe weather events, and other local weather changes. Additionally, high resolution satellite data provided by SPoRT has been used by the private sector to inform the marine weather community of changing ocean conditions and with tropical storm and hurricane monitoring. Because of its unique ability to transition NASA technologies into NOAA/NWS operations, the SPoRT Center is an ideal organization to participate in the annual Spring Experiments and provide feedback from both an operational and research perspective.

## 3. SPORT CENTER AND NSSL COLLABORATION

There is a long history of close interaction between meteorological researchers and operational weather forecasters in Norman, Oklahoma — a tradition that provides a fitting backdrop for the NOAA Hazardous Weather Testbed (HWT). This testbed emerged from a

*Corresponding author address:* Jonathan Case, ENSCO, Inc., 320 Sparkman Dr., Room 3062, Huntsville, AL, 35805. Email: Jonathan.Case-1@nasa.gov

grassroots level after the NOAA/NWS/Storm Prediction Center (SPC) moved its operations to Norman's NSSL facility in 1997. It was facilitated by the mutual interests of forecasters from the SPC and researchers from NSSL and inspired by the culture of collaboration that already existed in the Norman meteorological community.

The flagship activity for the emerging HWT was the annual SPC/NSSL Spring Experiment (formerly known as the Spring Program). Currently, this experiment attracts 50–60 researchers and forecasters from a variety of NOAA agencies, universities, and the private sector. It has been invigorated by formal collaboration and institutional support from the National Center for Environmental Prediction (NCEP) Environmental Modeling Center, the Center for Analysis and Prediction of Storms, the National Center for Atmospheric Research, and the NOAA Earth System Research Laboratory. It draws strength from its unique framework that provides forecasters with a first-hand look at promising new research concepts and products, while immersing research scientists in the challenges, needs, and constraints of front-line forecasters.

The meteorological community in Huntsville, AL also has a rich history of collaboration between researchers and practitioners, and in recent years there has been a concerted effort to draw the parallel and mutual interests of the Norman and Huntsville meteorological communities together. With expertise in lightning, numerical weather prediction, land surface modeling, air quality, and technology transition, along with the NASA presence at the Marshall Space Flight Center, the Huntsville meteorological community provides a valuable complementary perspective to research and operations in the annual Spring Experiments.

In addition to the annual Spring Experiment, the focal point for this interaction has been a high-resolution, real-time WRF modeling system, which has been operating since late 2006. The real-time forecasts provide an area of intense mutual interest for model developers and forecasters and they also provide overlapping research opportunities for research scientists in both communities. This effort has provided a compelling proof of concept that such a collaborative modeling effort can be very effective at creating a valuable synergy between groups of meteorologists that come from different agencies and are diverse in both focus and physical location.

## 4. THE OPERATIONAL NSSL WRF

The NSSL real-time forecasts employ the ARW dynamical core (Skamarock *et al.* 2005) from version 2.2 of the WRF public release, and are generated on a 64-processor SGI Altix 3700 computing system. The domain covers all but the westernmost portion of the Continental U.S. (Figure 1), consisting of 4-km horizontal grid spacing with 35 sigma-pressure vertical levels extending from the surface to 50 hPa at the domain top.

The ARW physics options consist of the rapid radiative transfer model (Mlawer *et al.* 1997) and the Dudhia scheme (Dudhia 1989) for longwave and shortwave radiation, respectively. The WRF Single Moment 6-class microphysics scheme (WSM6, Hong and Lim 2006; Skamarock *et al.* 2005) is used without any convective parameterization. The planetary boundary layer and turbulence processes are parameterized by the Mellor-Yamada-Janjić scheme (Janjić 1990, 1996, 2002). Land surface processes are handled by the Noah land surface model (LSM, Ek *et al.* 2003) while surface-layer calculations of friction velocities and exchange coefficients are provided by the NCEP Eta similarity theory scheme (Janjić 1996, 2002).

Daily ARW predictions are initialized and forced at the boundaries with the 0000 UTC NCEP North American Mesoscale (NAM) model data projected on a 40-km grid. The 40-km NAM data are interpolated to the WRF grid and boundaries using the WRF Pre-processing System (WPS) utilities. The NSSL runs are integrated out 36 h every day with forecasts typically completed by 0930 UTC. Output is provided directly to forecasters at the NOAA/Storm Prediction Center and several local NWS forecasting offices including Huntsville. Post-processing proceeds simultaneously with the model integration to help ensure the timeliness and relevance of the output to operational forecasters. The NSSL WRF output is also posted to the following website: http://www.nssl.noaa.gov/wrf/.

## 5. SENSITIVITY EXPERIMENT DESIGN

The experiment design is to run variations of the NSSL WRF simulations using NASA assets in order to demonstrate possible improvements in forecast accuracy. The GSFC has developed and implemented a 3-ice microphysics, shortwave, and longwave radiation physics packages into the ARW. The new GSFC physics schemes implemented into the ARW are described in detail in the following sub-sections.

### *5.1 GSFC Shortwave and Longwave Radiation*

The GSFC shortwave and longwave radiation schemes have been recently incorporated into the ARW (Matsui *et al.* 2007). This scheme is the up-to-date version of Goddard radiation scheme (Chou and Suarez 1999; Chou *et al.* 2001). The shortwave scheme fully accounts for the absorption due to water vapor, $O_3$, $O_2$, $CO_2$, clouds, and aerosols as well as for the scattering due to molecular, clouds, aerosols, and surface over 11-subdivided shortwave bands. Given the optical properties, fluxes are computed using the two-stream adding approximation. The longwave scheme accounts for the absorptions due to water vapor, $O_3$, $CO_2$, $N_2O$, $CH_4$, CFC's, clouds, and aerosols as well as for the scattering due to clouds and aerosols over 10-subdivided longwave bands. In comparison with a detailed line-by-line model, the atmospheric shortwave heating and longwave cooling rates between 0.01 hPa and the surface is accurate to within 5% and 7.5%, respectively (Chou and Suarez 1999; Chou *et al.* 2001). The GSFC shortwave and longwave radiation codes have been further developed for WRF applications by

- Optimizing the shortwave radiation code for computational speed (by a factor of two),

- Ensuring that cloud optical properties are consistent to the assumption in Goddard microphysics, and
- Including the option of adding stratospheric layers above the top of the model pressure level (Matsui *et al.* 2007).

### *5.2 GSFC Microphysics and the ARW WSM6*

The Goddard microphysical scheme (Tao *et al.* 2003), a one-moment bulk microphysical scheme recently incorporated into the WRF, is mainly based on Lin *et al.* (1983) with additional processes from Rutledge and Hobbs (1984). However, the Goddard microphysical scheme has several modifications. First, there is an option to choose either graupel or hail as the third class of ice (McCumber *et al.* 1991). Graupel has a relatively low density and a high intercept value (i.e., more numerous small particles). In contrast, hail has a relative high density and a low intercept value (i.e., more numerous large particles). These differences can affect not only the description of the hydrometeor population and formation of the anvil-stratiform region but also the relative importance of the microphysical-dynamical-radiative processes. Second, a new saturation technique (Tao *et al.* 1989) was added. This saturation technique is designed to ensure that super saturation (sub-saturation) cannot exist at a grid point that is clear (cloudy). Third, all microphysical processes that do not involve melting, evaporation or sublimation (i.e. transfer rates from one type of hydrometeor to another) are calculated based on one thermodynamic state. This ensures that all of these processes are treated equally. The opposite approach is to have one particular process calculated first modifying the temperature and water vapor content (i.e. through latent heat release) before the next process is computed. Fourth, the sum of all sink processes associated with one species will not exceed its mass. This ensures that the water budget will be balanced in the microphysical calculations. In addition to the two different three-ice schemes (i.e., cloud ice, snow and graupel or cloud ice, snow and hail), the Goddard microphysical scheme has a third option, which is equivalent to a two-ice scheme having only cloud ice and snow. This option may be needed for coarse resolution simulations (i.e., > 5 km grid size). The two-class ice scheme could be applied for winter and frontal convection; however, it is not explored in this study.

The WSM6 scheme also has five classes of hydrometeors, but with the revised ice microphysics proposed by Hong *et al.* (2004). The most distinguishing features of the Hong *et al.* (2004) are that (1) it practically represents ice microphysical processes by assuming the ice nuclei number concentration to be a function of temperature, (2) it involves the new assumption that the ice crystal number concentrations are a function of the amount of ice, and (3) it includes cloud ice sedimentation. The related ice processes are changed accordingly. The saturation adjustments are based on Tao *et al.* (2003) and separately treat the ice and water saturation processes. Hong *et al.* (2004) showed that significant improvements were made in high cloud amount, surface precipitation, and large-scale mean temperature through better representation of the ice-radiation feedback. A detailed description of the WSM6 scheme, including all the source/sink terms and the computational procedures, is given in Hong and Lim (2006).

### *5.3 SPoRT MODIS SSTs*

Additional sensitivity experiments include the SPoRT Center high-resolution (2-km) MODIS SST composite for representing water temperatures in the ARW (Haines *et al.* 2007; LaCasse *et al.* 2008). To incorporate the MODIS SST composites into the ARW runs, the SST data are simply interpolated onto the WRF grid using the WPS utilities, and are held constant for the duration of the simulation. The skin temperatures over water grid points are thus replaced with the high-resolution SPoRT SST data.

### *5.4 LIS Initialization of the Land Surface*

Finally, sensitivity experiments are conducted using land surface initialization data from the NASA LIS. Previous work by Case *et al.* (2008) has demonstrated the positive impact of a properly spun-up land surface model within LIS to initialize WRF forecasts over the Florida region. These sensitivity experiments seek to extend their work to severe convective cases to determine the possible improvements in convective initiation and evolution due to a high-resolution spin-up of the land surface variables.

The Noah LSM is run offline within the NASA LIS for a long integration period (i.e. 4+ years) in order to provide the WRF with soil variables in an equilibrium state. For the offline simulation, version 2.7.1 of the Noah LSM is run in LIS version 5 on the exact horizontal grid configuration of the NSSL WRF, with the same soil and vegetation database as used by WRF. For the sensitivity simulations presented in this paper, atmospheric forcings for the LIS run are provided by the Global Data Assimilation System analyses (GDAS; Derber *et al.* 1991), which consist of three-hourly analyses at a horizontal resolution of 0.469° (~52 km).

Spinning up the soil model on the exact WRF horizontal grid is important because it ensures consistency between the initial soil variables and the soil properties represented at each grid point (e.g. soil porosity, hydraulic conductivity, etc.). Interpolation of soil fields from larger-scale model data (such as the operational NCEP NAM) can lead to mis-representations of the initial soil temperature and moisture in the high-resolution WRF initial conditions due to resolution and grid mis-matches.

### *5.5 Customized Model Products for the SPC*

Guidance from numerical weather prediction models is typically presented as a series of snapshots in time (an exception is accumulated precipitation). Traditionally, this has been adequate for most applications because common features of interest evolve slowly compared to the time between outputs. Furthermore, the path followed by these features can be implied with reasonable precision by assuming temporal continuity between output times. However, output in this format can leave many questions unanswered when the phenomena of interest develop, move, and vary in intensity on times scales shorter than the output frequency. Under these circumstances, it can be useful (while remaining computationally efficient) to track features or phenomena of interest every time step during the model integration, and then plot the average or extreme values of the data at regular output intervals.

In collaborations between scientists at the NOAA/NSSL and forecasters at the NOAA/NWS/Storm Prediction Center, this concept was applied in mesoscale models several years ago. For example, upward mass flux in parameterized convective updrafts was checked at each grid point, every time step, and the maximum value at each point was saved at normal output intervals. The 2-D field of grid-point maxima provided unique information about the magnitude of parameterized convective overturning, which in turn provided useful guidance for the intensity of convective activity in the real atmosphere (Kain *et al.* 2003).

Recently, this concept is applied to the real-time convection-allowing forecasts at NSSL. In particular, it is used to extract sub-output-time information about convective storms in the model, initially focusing on five different output fields. The first two are maximum updraft and downdraft velocities in the lowest 400 hPa of the model atmosphere. These two fields have obvious implications regarding the intensity of convective overturning. The third field is maximum simulated reflectivity. For simplicity, this is computed at the lowest model level, but without much additional computational effort, other levels (or a composite) could be used. As with updraft and downdraft velocities, this field is related to the intensity of convection and may provide some guidance for forecasting large hail, even though hail is not explicitly represented in the WSM6 microphysical scheme. The fourth field is maximum 10-m wind speed, which may be helpful in predicting the magnitude of convectively induced wind gusts. The last field is maximum updraft helicity, a diagnostic field that was developed before the 2005 HWT Spring Experiment to detect mid-level mesocyclones in simulated convection (see Kain *et al.* 2008).

While these fields are useful for diagnosing maximum values, valuable clues about storm tracks, wind swaths, and the longevity of individual features also are provided. For example, on several days this spring the 4-km NSSL WRF model produced long-lived (multi-hour), strongly rotating mesocyclones that were revealed in hourly output as downstream-marching segments of high maximum updraft helicity. With relatively simple post-processing tools, one can concatenate such segments to reveal features such as storm tracks or wind swaths.

## 6. PRELIMINARY RESULTS: IMPACTS OF NASA PHYSICS ON 28 MAR 2007 CASE

This section focuses on preliminary results from the 28 March 2007 severe weather outbreak. In this event, there were 80 tornado and 198 severe hail reports ranging from the Texas Panhandle north to western Nebraska (Figure 2). Much of this activity occurred after 2200 UTC 28 March, as a strong upper-level trough approached the western High Plains (not shown).

A series of tornadoes occurred across the southern and eastern Texas Panhandle associated with supercell thunderstorms that rapidly developed between 2200 and 2300 UTC 28 March (Figure 3a-b), and continued northward across the eastern Texas Panhandle through 0300 UTC (Figure 3c-f). A squall line then developed across western Texas and progressed eastward from 0200 UTC to 0500 UTC (Figure 3e-h). Other tornadic storms occurred along the Colorado/Kansas border into western Nebraska generally after 0000 UTC 29 March (reports in Figure 2; radar images not shown).

One feature noted in the real-time NSSL WRF runs for this case is the under-forecast of the severe convection coverage and intensity. Our NSSL co-author noted that the 4-km real-time NSSL WRF under-developed convective activity because it could not dissipate the boundary-layer-topped clouds and never developed adequate surface heating over initiation zones. Two-meter temperatures were subsequently too cold and 2-m dewpoints somewhat high.

Based on the suite of sensitivity experiments conducted for this case day, the runs with the new GSFC shortwave radiation scheme (hereafter gsfcsw; not available in the public WRF version) had the greatest impact on the simulated 2-m temperatures, cloud cover, and subsequent convection for the 28 March case. Therefore, the results presented in this paper focus on the differences between the Control run (i.e. real-time NSSL WRF) and the gsfcsw run. The poster presents some comparisons of the other sensitivity runs, but these differences were generally small compared to the impacts of the gsfcsw.

The simulated 2-m temperature field at 2100 UTC 28 March (just prior to convective initiation over the Texas Panhandle) depicted a large warm sector across much of the Southern Plains into southwestern Iowa and Nebraska. A band of relatively cooler 2-m temperatures ranging from ~12°C to 20°C were predicted in the Control run (i.e. real-time NSSL WRF configuration) from western Oklahoma into northwestern Nebraska (Figure 4a). In the gsfcsw run, the predicted 2-m temperatures were considerably warmer along this corridor, generally 1–4°C greater than the Control run (Figure 4b-c). These temperatures were qualitatively closer to the observed values at 2100 UTC (Figure 4d).

The warmer temperatures in the gsfcsw run were a manifestation of the reduced total cloud cover in the model. The 21-hour forecast total cloud condensate depicted both reduced total condensate amount and areal coverage, especially over western Nebraska and northern Kansas (Figure 5). The result of the reduced cloud cover and increased 2-m temperatures was a substantial increase in the simulated convective available potential energy (CAPE) at 2100 UTC (Figure 6).

The development and evolution of deep convection in the gsfcsw run was subsequently more intense over the entire initiation region from the eastern Texas Panhandle/western Oklahoma, northward into Nebraska. Figure 7 through Figure 11 depict the differences in hourly convective evolution across the Southern Plains portion of the NSSL forecast domain from 2100 UTC 28 March to 0100 UTC 29 March. Each figure includes the forecast composite reflectivity (maximum column at model output time) for the Control and gsfcsw runs in panels a and b, and the hourly maximum base reflectivity (BREF) at the first WRF model vertical level from the previous hour, as described in Section 5.5.

At valid time 2100 UTC, the Control run has scattered convective activity developing across far western Nebraska and lighter activity over the eastern Texas Panhandle (Figure 7a,c). The gsfcsw run depicts a similar pattern of convective activity, but with slightly more intense and larger cells over the eastern Texas Panhandle (Figure 7b,d). By 2200 UTC, the gsfcsw run has markedly more intense convection over extreme western Oklahoma, and a reduced coverage of light reflectivity over central Nebraska and Kansas, coinciding with the reduced cloud cover in those regions (Figure 8). At 2300 UTC, stronger cells continue in western Oklahoma in the gsfcsw simulation, with additional cells developing in the eastern Texas Panhandle (Figure 9b,d), in the region where tornadic supercells occurred (Figure 3c). The Texas Panhandle activity in the Control run was much less prevalent at this time (Figure 9a,c). The maximum hourly BREF plots in Figure 9c and d clearly indicate the more intense cells tracking to the north-northeast over Oklahoma/Texas up to northwestern Nebraska. By 0000 UTC 29 March, the gsfcsw run still depicts much more intense convection in the Texas and Oklahoma Panhandles compared to the Control run (Figure 10). Not until 0100 UTC does the Control run begin to generate convection of similar intensity to the gsfcsw run (Figure 11). Even so, the gsfcsw still depicts cells with more supercellular structure than in the Control, closer to the observed activity in the Texas Panhandle. Analysis of the heating rates within the GSFC and Dudhia shortwave schemes is needed to help determine the major contributing factor(s) that allowed the new GSFC shortwave scheme to thin out the boundary layer clouds more than in the Control.

Other sensitivity runs not shown in this paper generally had small or slightly negative impact on the forecast convection for this case. The GSFC longwave radiation scheme generally had nominal impacts, but with a slight cooling effect on the 2-m temperatures compared to the Control run. The GSFC microphysics runs had even more trouble clearing out the boundary layer cloudiness, and resulted in cooler temperatures, less instability, and less widespread/intense convection. The LIS land surface initialization (lisic) provided higher-resolution soil information consistent with the WRF grid resolution (i.e. 0–10 cm initial soil moisture comparison in Figure 12); however, for this particular case, the LIS initialization did not have much impact on the convective development and evolution. Also, the soil moisture and temperature fields appeared to be mis-represented in portions of the Rockies, probably due to the lack of an elevation correction between the coarse-resolution GDAS atmospheric forcing data and the high-resolution LIS grid elevation. The MODIS SST sensitivity test was not conducted for this case day yet.

## 7. SUMMARY AND FUTURE WORK

This paper presented an experiment design for conducting sensitivity tests for selected severe weather cases to determine the impacts of unique NASA physics and datasets on subsequent WRF forecasts on the real-time NSSL domain. Selected results were presented from the 28 March 2007 High Plains tornado outbreak, highlighting some improvements that resulted from using the new GSFC shortwave radiation physics scheme not available in the current public WRF. The GSFC shortwave scheme produced more accurate 2-m temperature predictions that led to increased CAPE, and more intense convection near the region where observed tornadic supercells occurred in the eastern Texas Panhandle to western Nebraska.

Future work will involve diagnosing the physical mechanisms in the GSFC shortwave radiation scheme that were responsible for producing better results from the 28 March 2007 case study compared to the Control simulation using the Dudhia shortwave radiation. In addition, the remaining selected cases from the 2007 Spring Experiment, as well as additional cases from the Spring 2008 severe weather season, will be examined, including sensitivity tests with MODIS SSTs.

Future LIS/WRF sensitivity runs on the NSSL domain will utilize higher-resolution atmospheric forcing from the North American Land Data Assimilation System (NLDAS, Cosgrove *et al.* 2003; Mitchell *et al.* 2004), which consists of hourly analyses at 0.125° (~14 km) horizontal resolution, as well as GDAS forcing with elevation corrections to the LIS grid. Such improvements to the LIS will result in more accurate spatial variations of the soil temperature and moisture in the Rockies and Mexico due to the elevation correction, and in all areas in the Continental U.S. with the addition of the NLDAS forcing.

## 8. ACKNOWLEDGEMENTS/DISCLAIMER

This research was funded by Dr. Tsengdar Lee of the NASA Science Mission Directorate's Earth Science Division in support of the SPoRT program at the NASA Marshall Space Flight Center. Computational resources for this work were provided by the NASA Center for Computational Sciences at the NASA Goddard Space Flight Center.

Mention of a copyrighted, trademarked or proprietary product, service, or document does not constitute endorsement thereof by the authors, ENSCO Inc., the SPoRT Center, the National Aeronautics and Space Administration, the National Severe Storms Laboratory, or the United States Government. Any such mention is solely for the purpose of fully informing the reader of the resources used to conduct the work reported herein.

## 9. REFERENCES

Case, J. L., W. L. Crosson, S. V. Kumar, W. M. Lapenta, and C. D. Peters-Lidard, 2008: Impacts of High-Resolution Land Surface Initialization on Regional Sensible Weather Forecasts from the WRF Model. *Accepted in J. Hydrometeor.*

Chou, M.-D., and M. J. Suarez, 1999: A solar radiation parameterization for atmospheric studies. NASA Tech. Pre. NASA/TM-1999-10460, vol. 15, 38 pp.

Chou, M.-D., M. J. Suarez, X-Z. Liang, and M. M.-H. Yan, 2001: A thermal infrared radiation parameterization for atmospheric studies. NASA/TM-2001-10406, vol. 19, 55 pp.

Cosgrove, B. A., and Coauthors, 2003: Real-time and retrospective forcing in the North American Land Data Assimilation System (NLDAS) project, *J. Geophys. Res.,* **108(D22),** 8842, doi:10.1029/2002JD003118, 2003.

Derber, J. C., D. F. Parrish, and S. J. Lord, 1991: The new global operational analysis system at the National Meteorological Center. *Wea. Forecasting,* **6,** 538-547.

Dudhia, J., 1989: Numerical study of convection observed during the winter monsoon experiment using a mesoscale two-dimensional model. *J. Atmos. Sci.,* **46,** 3077-3107.

Ek, M. B., K. E. Mitchell, Y. Lin, E. Rogers, P. Grunmann, V. Koren, G. Gayno, and J. D. Tarpley, 2003: Implementation of Noah land surface model advances in the National Centers for Environmental Prediction operational mesoscale Eta model. *J. Geophys. Res.,* **108 (D22),** 8851, doi:10.1029/2002JD003296.

Haines, S. L., G. J. Jedlovec, and S. M. Lazarus, 2007: A MODIS sea surface temperature composite for regional applications. *IEEE Trans. Geosci. Remote Sens.,* **45,** 2919-2927.

Hong, S.-Y., J. Dudhia, and S.-H. Chen, 2004: A revised approach to ice microphysical processes for the bulk parameterization of clouds and precipitation, *Mon. Wea., Rev.,* **132**, 103-120.

Hong, S.-Y., and J-O J. Lim, 2006: The WRF single-moment 6-class microphysics scheme (WSM6). *J. Korean Meteor. Soc.,* **42,** 129-151.

Janjić, Z. I., 1990: The step-mountain coordinate: Physical package. *Mon. Wea. Rev.,* **118,** 1429–1443.

Janjić, Z. I., 1996: The surface layer in the NCEP Eta Model. Preprints, *Eleventh Conference on Numerical Weather Prediction,* Norfolk, VA, Amer. Meteor. Soc., 354–355.

Janjić, Z. I., 2002: Nonsingular Implementation of the Mellor–Yamada Level 2.5 Scheme in the NCEP Meso model, NCEP Office Note, No. 437, 61 pp.

Kain, J. S., M. E. Baldwin, and S. J. Weiss, 2003: Parameterized updraft mass flux as a predictor of convective intensity. *Wea. Forecasting,* **18**, 106-116.

Kain, J. S., S. J. Weiss, D. R. Bright, M. E. Baldwin, J. J. Levit, G. W. Carbin, C. S. Schwartz, M. L. Weisman, K. K. Droegemeier, D. B. Weber, K. W. Thomas, 2008: Some practical considerations regarding horizontal resolution in the first generation of operational convection-allowing NWP. *Wea. Forecasting,* in press.

Kumar, S. V., and Coauthors, 2006. Land Information System – An Interoperable Framework for High Resolution Land Surface Modeling. *Environmental Modeling & Software,* **21 (10),** 1402-1415, doi:10.1016/j.envsoft.2005.07.004.

Kumar, S. V., C. D. Peters-Lidard, J. L. Eastman, and W.-K. Tao, 2007: An integrated high-resolution hydrometeorological modeling testbed using LIS and WRF. *Environmental Modeling & Software,* **23 (2),** 169-181, doi: 10.1016/j.envsoft.2007.05.012.

LaCasse, K. M., M. E. Splitt, S. M. Lazarus, and W. M. Lapenta, 2008: The impact of high-resolution sea surface temperatures on the simulated nocturnal Florida marine boundary layer. *Mon. Wea. Rev.,* **136,** 1349-1372.

Lin, Y.-L., R. D. Farley and H. D. Orville, 1983: Bulk parameterization of the snow field in a cloud model. *J. Clim. Appl. Meteor.*, **22**, 1065-1092.

Matsui, T., W.-K. Tao, and J.-J. Shi, 2007: Goddard radiation and aerosol direct effect in Goddard WRF. NASA/UMD WRF meeting, College Park, MD, Sep 14, 2007.

McCumber, M., W.-K. Tao, J. Simpson, R. Penc, and S.-T. Soong, 1991: Comparison of ice-phase microphysical parameterization schemes using numerical simulations of tropical convection. *J. Appl. Meteor.*, **30**, 985-1004.

Mitchell, K. E., and Coauthors, 2004: The multi-institution North American Land Data Assimilation System (NLDAS): Utilization of multiple GCIP products and partners in a continental distributed hydrological modeling system. *J. Geophys. Res.,* **109,** D07S90, doi:10.1029/2003JD003823.

Mlawer, E. J., S. J. Taubman, P. D. Brown, M. J. Iacono, and S. A. Clough, 1997: Radiative transfer for inhomogeneous atmosphere: RRTM, a validated correlated-k model for the long-wave. *J. Geophys. Res.,* **102 (D14),** 16663-16682.

Rutledge, S.A., and P.V. Hobbs, 1984: The mesoscale and microscale structure and organization of clouds and precipitation in mid-latitude clouds. Part XII: A diagnostic modeling study of precipitation development in narrow cold frontal rainbands. *J. Atmos. Sci.*, **41**, 2949-2972.

Skamarock, W. C., J. B. Klemp, J. Dudhia, D. O. Gill, D. M. Barker, W. Wang and J. G. Powers, 2005: A Description of the Advanced Research WRF Version 2, NCAR Tech Note, NCAR/TN–468+STR, 88 pp. [Available from UCAR Communications, P.O. Box 3000, Boulder, CO, 80307; on-line at: http://box.mmm.ucar.edu/wrf/users/docs/arw_v2.pdf]

Tao, W.-K., J. Simpson and M. McCumber, 1989: An ice-water saturation adjustment. *Mon. Wea. Rev.*, **117**, 231-235.

Tao, W.-K., J. Simpson, D. Baker, S. Braun, M.-D. Chou, B. Ferrier, D. Johnson, A. Khain, S. Lang, B. Lynn, C.-L. Shie, D. Starr, C.-H. Sui, Y. Wang and P. Wetzel, 2003: Microphysics, Radiation and Surface Processes in a Non-hydrostatic Model, *Meteorology and Atmospheric Physics,* **82**, 97-137.

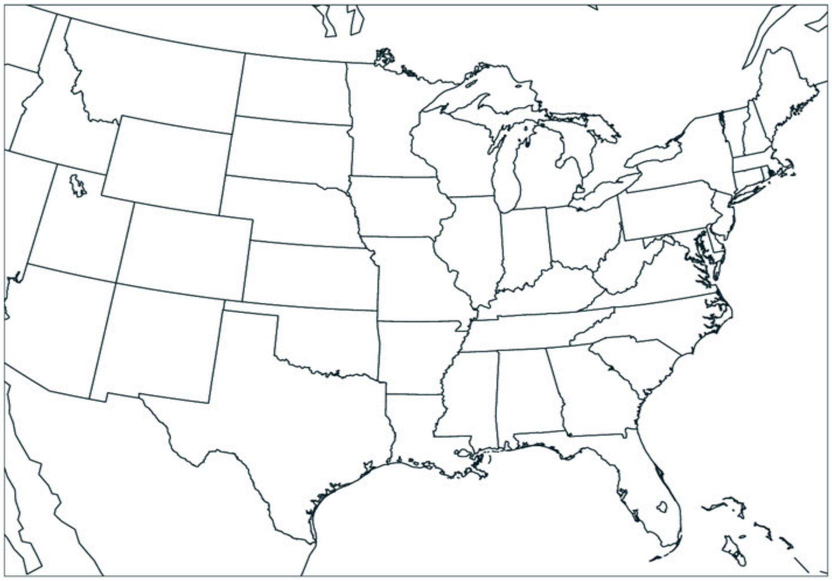

**Figure 1. Domain of the real-time NSSL WRF model.**

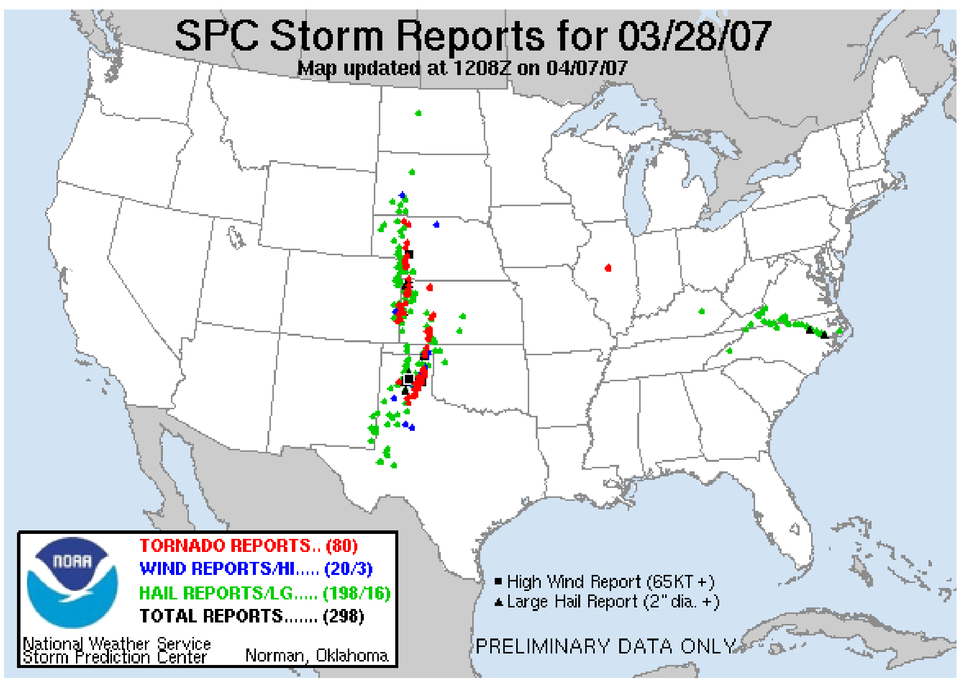


**Figure 2. Storm Prediction Center (SPC) archived severe weather reports for 28 March 2007.**

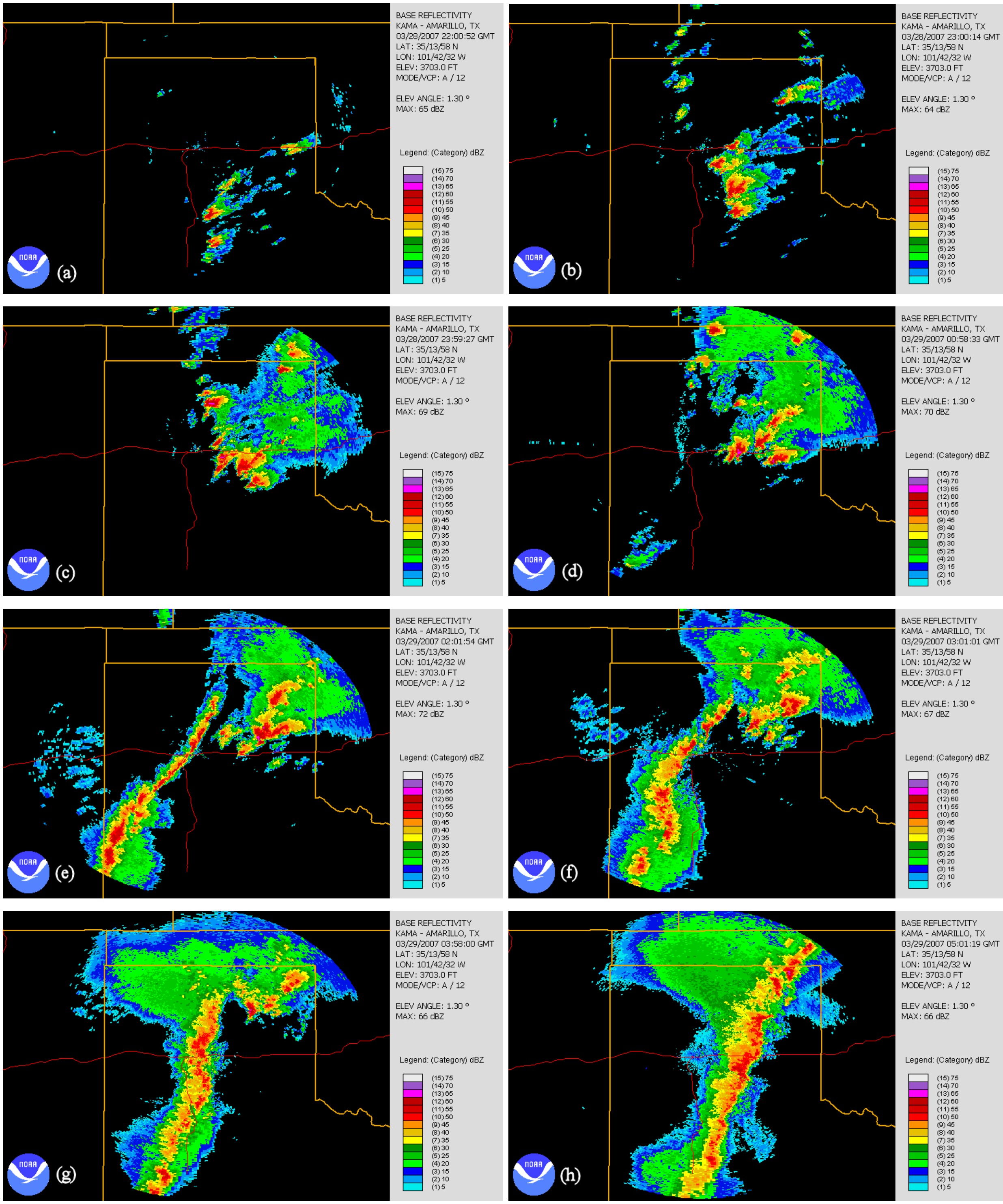


**Figure 3. Sequence of hourly Level III base reflectivity images from the Amarillo, TX WSR-88D valid at (a) 2200 UTC 28 March, (b) 2300 UTC 28 March, (c) 0000 UTC 29 March, (d) 0100 UTC 29 March, (e) 0200 UTC 29 March, (f) 0300 UTC 29 March, (g) 0400 UTC 29 March, and (h) 0500 UTC 29 March.**

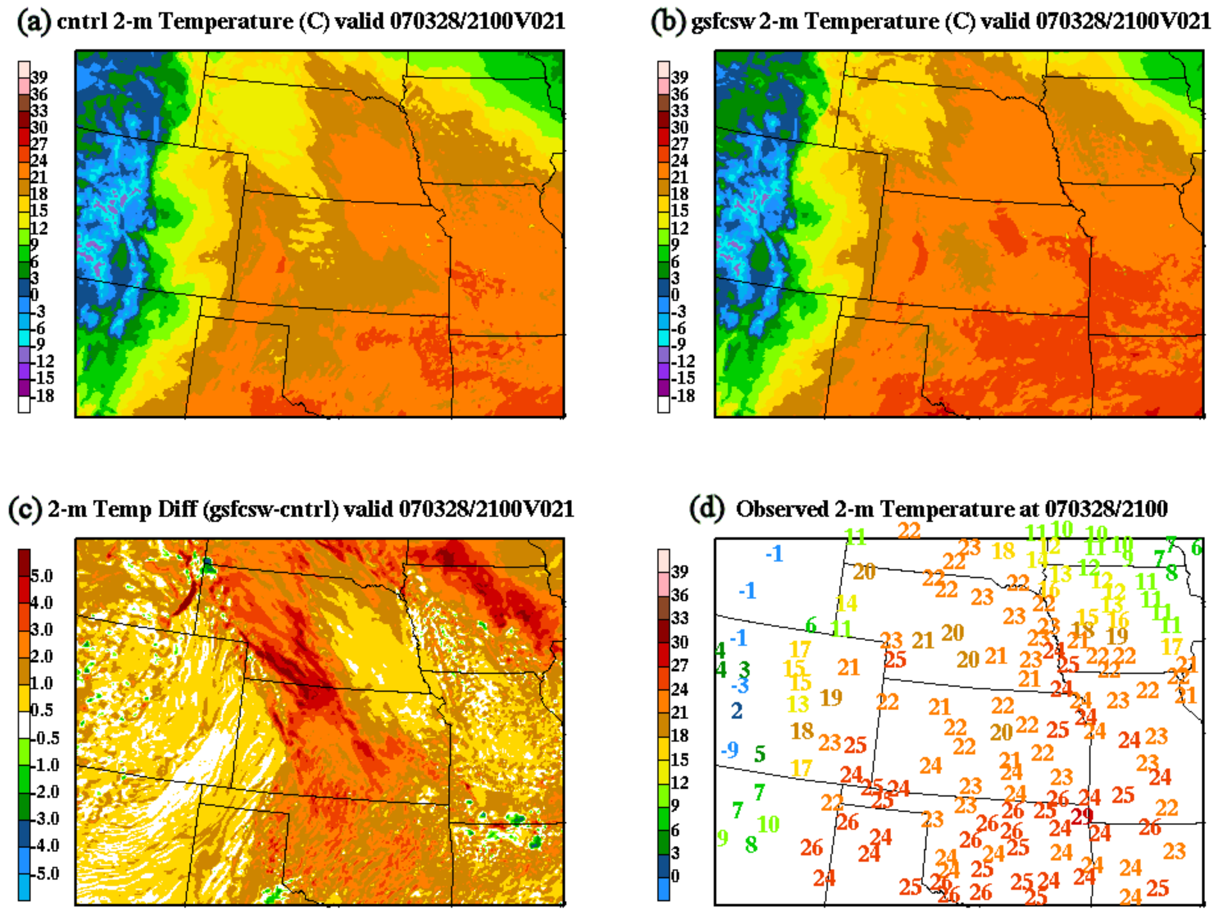


**Figure 4. WRF 21-hour forecast 2-m temperatures (°C) initialized at 0000 UTC 28 March 2007, for (a) the control run (cntrl), (b) Experimental run using the Goddard shortwave radiation scheme (gsfcsw), (c) Difference between the Control and gsfcsw, and (d) Observed 2-m temperatures at 2100 UTC.**

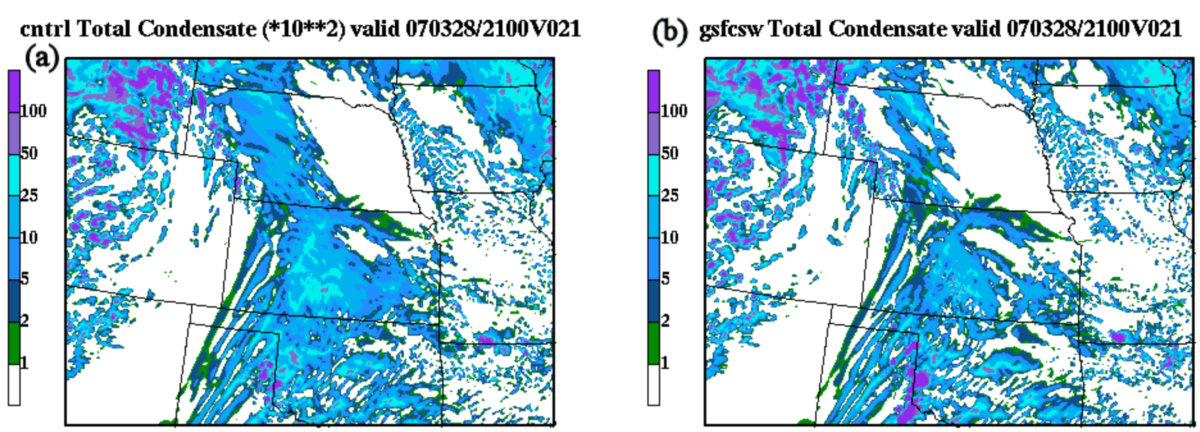


**Figure 5. WRF 21-hour forecast total column condensate (g kg$^{-1}$ x 10$^{2}$) initialized at 0000 UTC 28 March for (a) the control run, and (b) the gsfcsw run.**

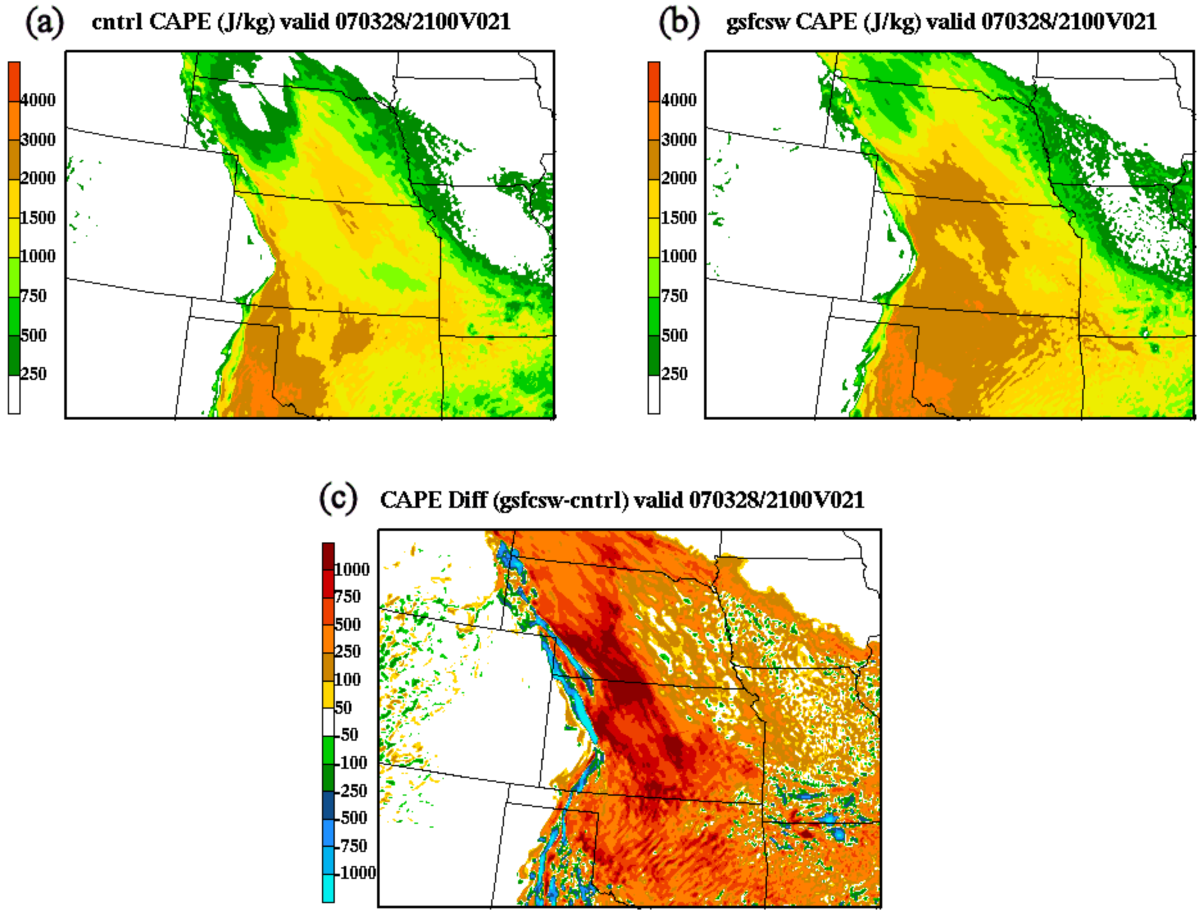


**Figure 6. WRF 21-hour forecast CAPE (J kg$^{-1}$) initialized at 0000 UTC 28 March 2007, for (a) the control run, (b) the gsfcsw, and (c) Difference between the Control and gsfcsw.**

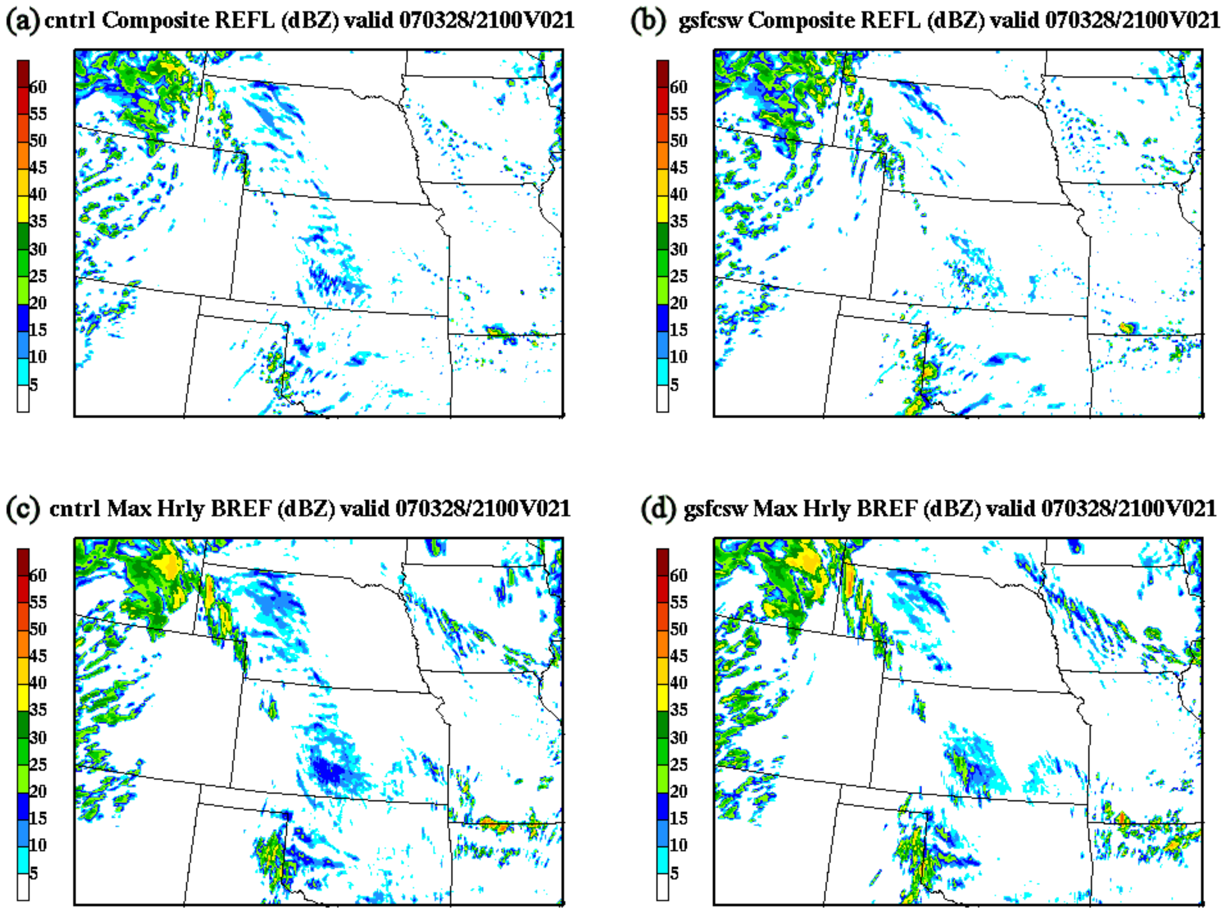


**Figure 7. WRF 21-hour forecast reflectivity (dBZ) valid at 2100 UTC 28 March 2007, for (a) the control run, (b) the gsfcsw run, (c) maximum hourly base reflectivity from the control run, and (d) maximum hourly base reflectivity from the gsfcsw run.**

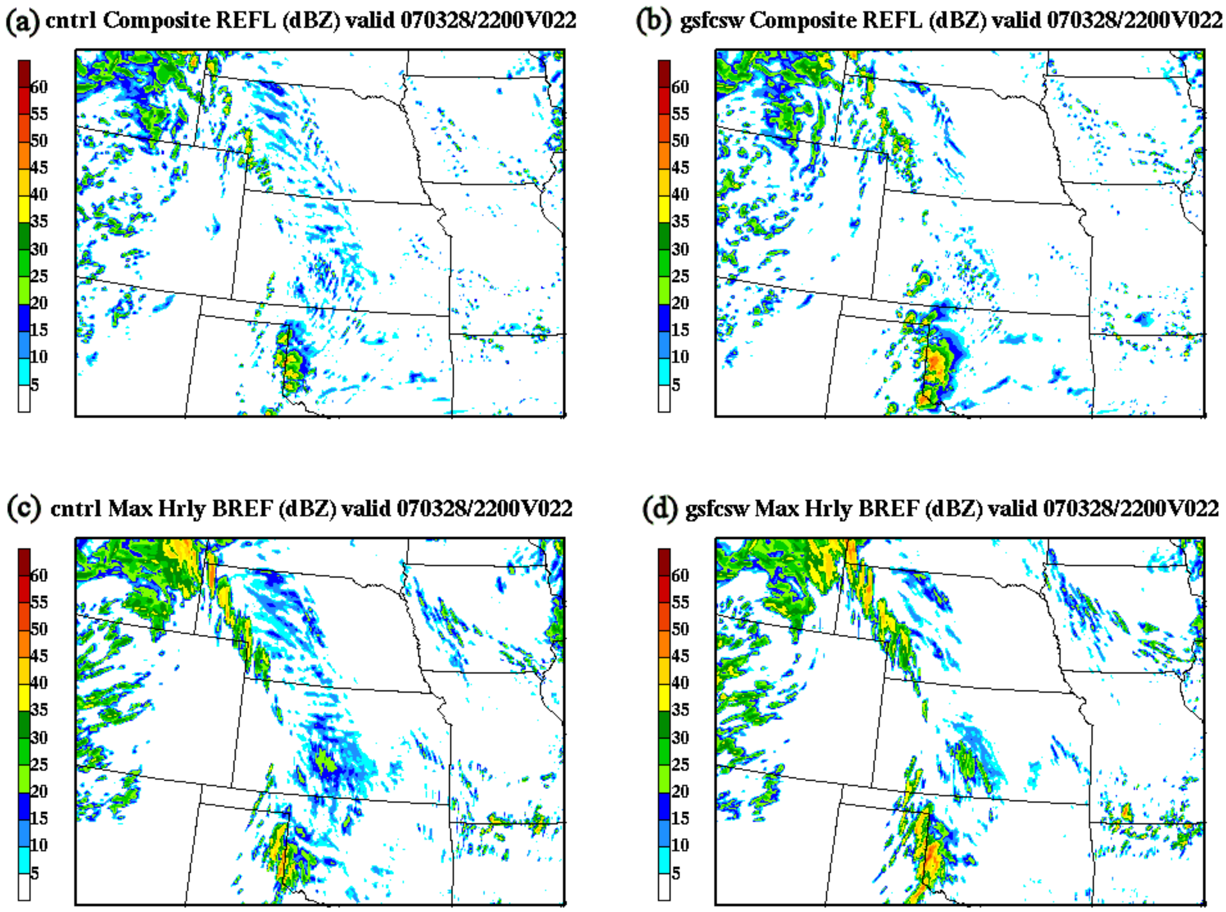


**Figure 8. Same as in Figure 7, except for the 22-hour forecast valid at 2200 UTC 28 March 2007.**

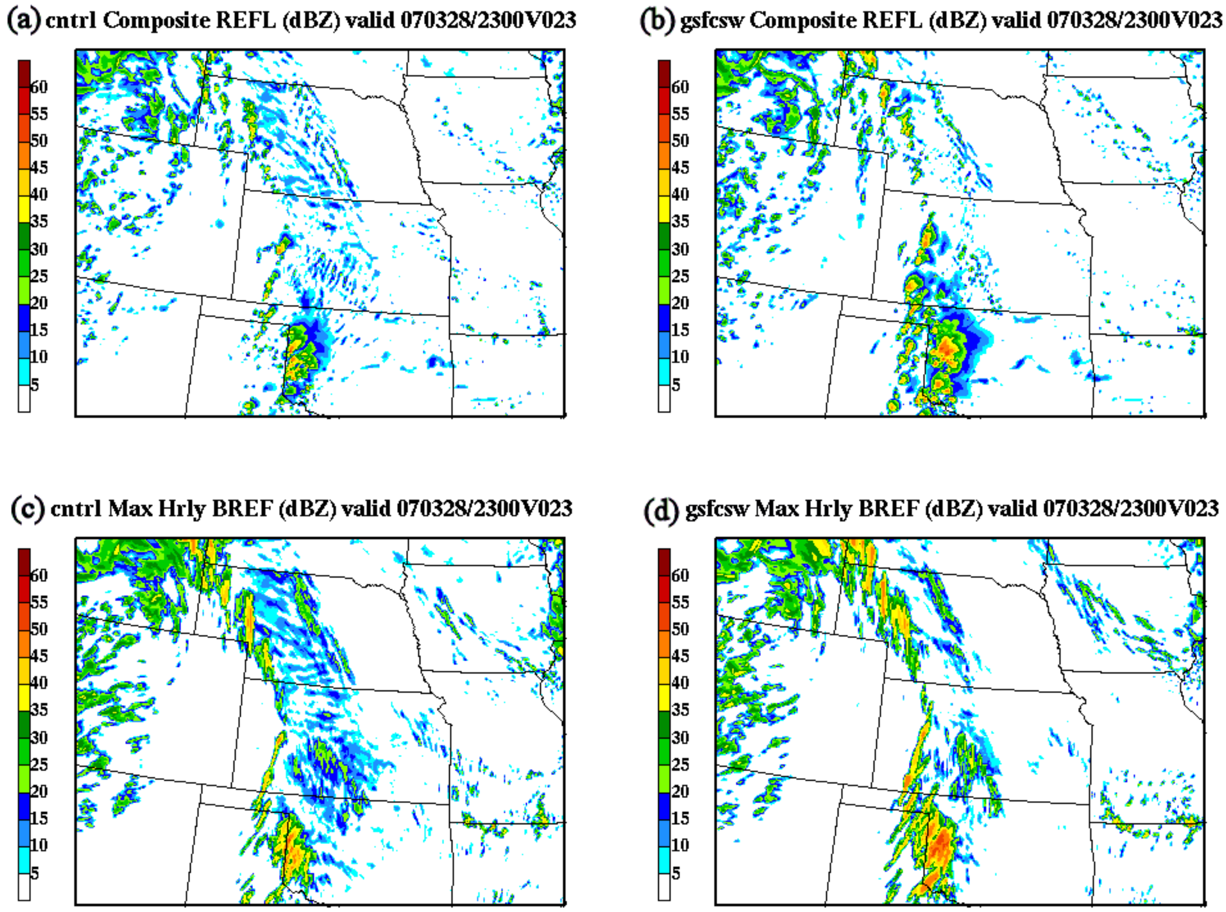


**Figure 9. Same as in Figure 7, except for the 23-hour forecast valid at 2300 UTC 28 March 2007.**

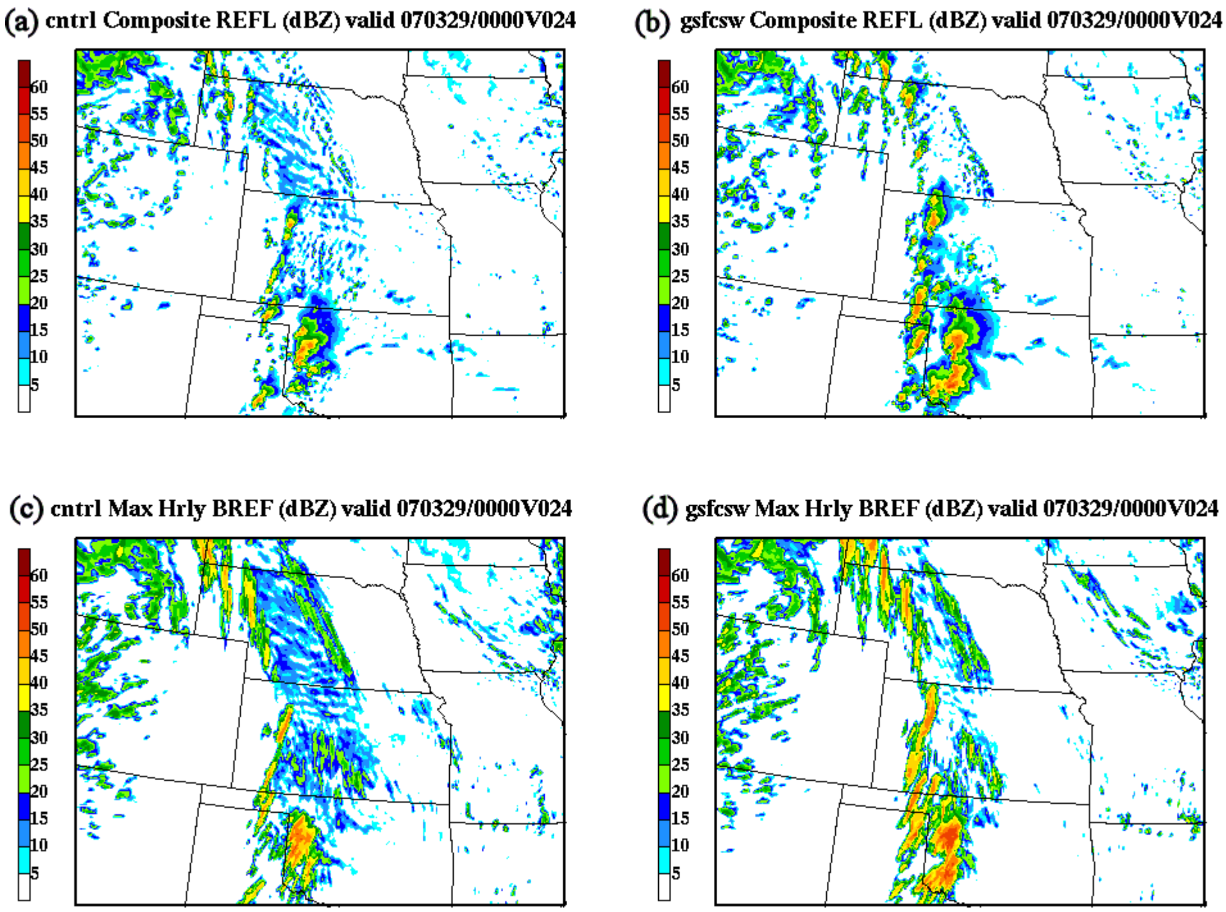


**Figure 10. Same as in Figure 7, except for the 24-hour forecast valid at 0000 UTC 29 March 2007.**

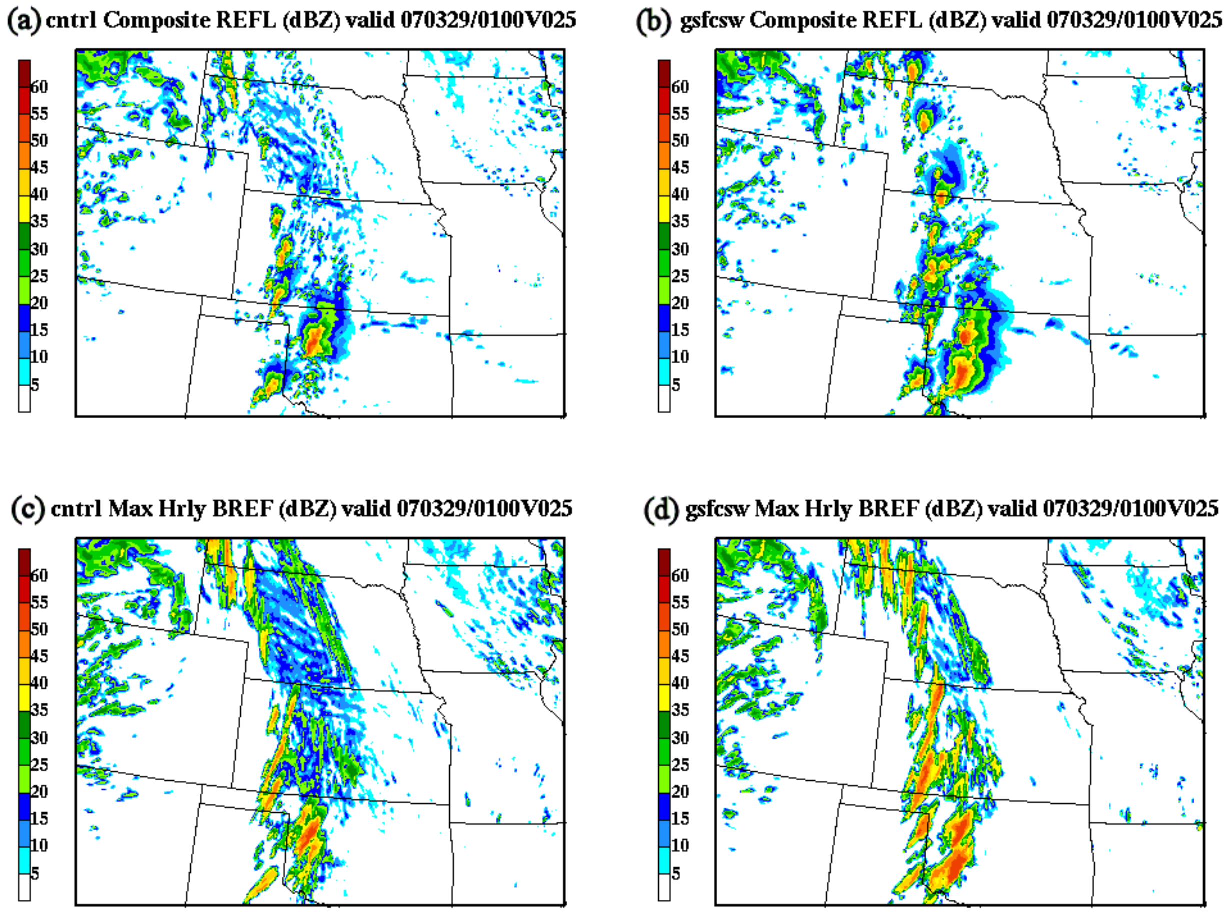


**Figure 11. Same as in Figure 7, except for the 25-hour forecast valid at 0100 UTC 29 March 2007.**

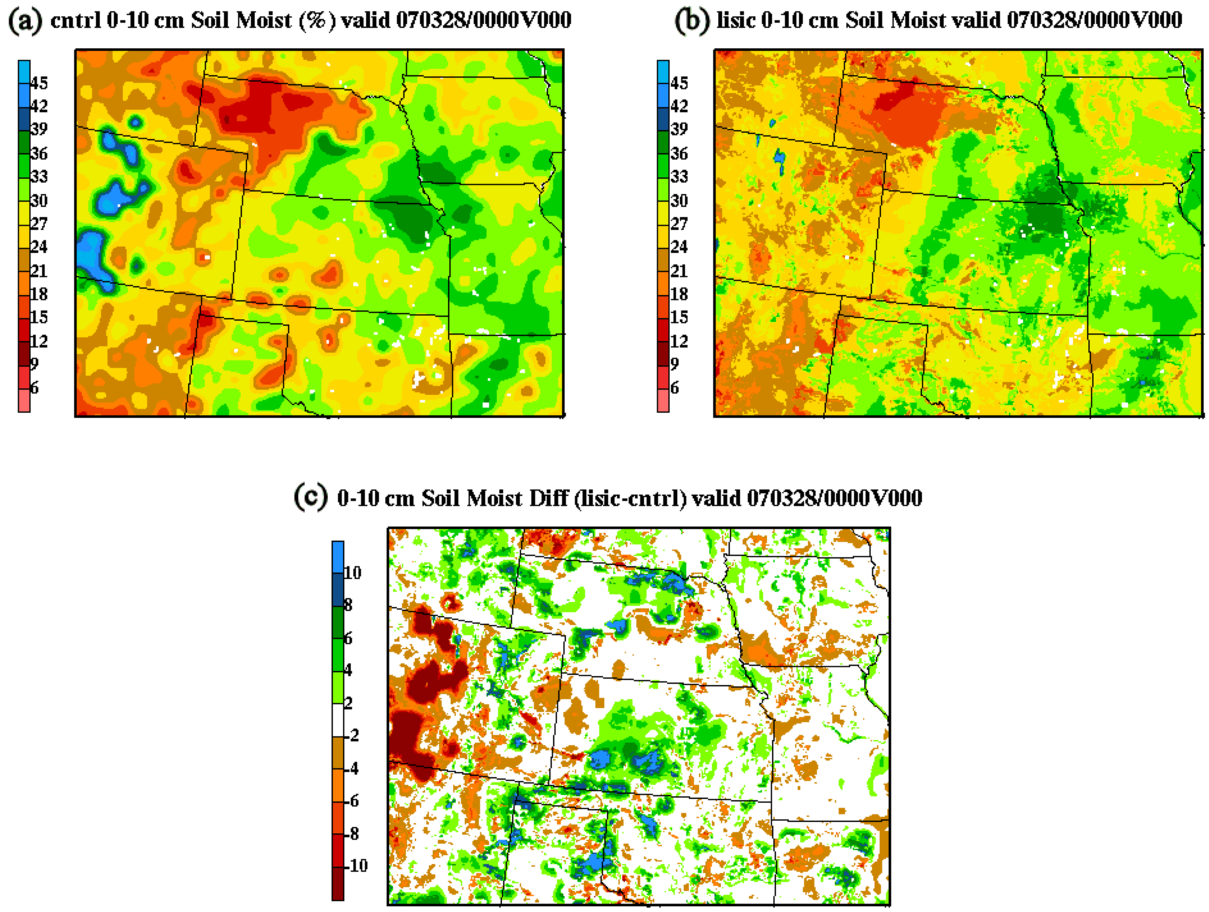


**Figure 12.** Initial 0–10 cm volumetric soil moisture (%) for the 0000 UTC 28 March 2007 WRF simulation for (a) the Control NSSL WRF interpolating soil moisture off of the 40-km NCEP NAM data, (b) the offline LIS run integrating the Noah land surface model from 1 Jan 2004 to 28 March 2007, and (c) the difference between the LIS and Control 0–10 cm initial soil moisture.